



## Rock lithological classification using multi-scale Gabor features from sub-images, and voting with rock contour information



Claudio A. Perez <sup>\*</sup>, Jacob A. Saravia, Carlos F. Navarro, Daniel A. Schulz, Carlos M. Aravena, Francisco J. Galdames

Image Processing Laboratory, Department of Electrical Engineering and Advanced Mining Technology Center, Universidad de Chile, Av. Tupper 2007, Santiago, Chile

### ARTICLE INFO

#### Article history:

Received 19 May 2014

Received in revised form 25 June 2015

Accepted 15 September 2015

Available online 3 October 2015

#### Keywords:

Rock classification

Lithological classification

Grindability estimation

Gabor feature extraction

Texture features

Feature selection

### ABSTRACT

Estimation of rock composition in mining plants is important for determining rock size and grindability which, in turn, may improve control of the grinding process. Variations in ore grindability and size distribution directly affect a mill's power consumption and throughput. It is therefore highly desirable to develop new methods to estimate rock lithological composition remotely. In this paper, a new method for remote lithological classification based on digital image analysis is proposed. The method is based on a single digital video camera for image acquisition from rocks on a conveyor belt. Each image is broken into sub-images to extract texture information using several different spatial scales. Gabor filters are used to extract features from each sub-image for five different spatial scales and eight orientations. After feature extraction, each sub-image is classified into a lithological class using a support-vector machine (SVM). Finally, information from the contour of each rock is used to select all sub-images that fall inside the contour and vote for the rock class. The method was tested on three databases, one of them containing sub-images of  $64 \times 43$  pixels of five ore types assigned to three grindability classes (soft, medium and hard). The second database has seven ore types containing sub-images of  $60 \times 40$  pixels. The third database was captured with higher resolution cameras and controlled illumination with five ore types and containing sub-images of  $64 \times 48$ . The databases were divided into 2 subsets, one for training with cross validation, and the other for testing. Classification accuracy was compared with previously published results on both databases. Comparisons show that our proposed method yielded significant improvements in classification accuracy, between 8.3% and 26%, relative to previously published results.

© 2015 Elsevier B.V. All rights reserved.

### 1. Introduction

In the mining industry, the problem of rock classification is important at different stages of the extractive process (Chatterjee et al., 2010b; Perez et al., 2011b, 2012). The rock type determines different process parameters such as grindability, slurry viscosity and screening efficiency, among others (Casali et al., 2001). Grindability characterization is usually performed off-line using a few ore samples to determine the hardness of the rocks (Morrell, 2004). This information can be used to control the mill operation. A reasonable online estimation of the rock hardness can improve the mill throughput and the power consumption (Tessier et al., 2007). New methods for online grindability characterization will have a great impact on reducing the energy costs of grinding mills because 55% of the total energy required in a mining operation is used in the grinding process (Buckingham et al., 2011). Therefore, a new methodology for online characterization of the ore at the mill input is a high priority.

In the past few years a relation has been established between ore variability and mineral processing. The proposed method could be used in future applications to improve ore characterization. This is particularly important in the field of geometallurgy. There is a need to understand better the ore variability to maximize the value from the ore (De Magalhães and Tavares, 2014; Yildirim et al., 2014; Mwanga et al., 2015).

Image analysis has been applied in several mining applications, such as online inspection of crushed aggregates (Al-Batah et al., 2009), diagnosis of surface chemical species (Gerson et al., 2012), online ore sorting and classification (Baykan and Yilmaz, 2010; Bianconi et al., 2012; Casali et al., 2001; Chatterjee et al., 2010a, 2010b; Chatterjee, 2012; Guyot et al., 2004; Köse et al., 2012; Mat Isa et al., 2011; Perez et al., 1999, 2011b; Shang and Barnes, 2012; Singh and Rao, 2006; Tessier et al., 2007), classification of electrical boreholes (Jungmann et al., 2011), particle and blast fragment size estimation and/or distribution (Al-Thyabat et al., 2007; Andersson et al., 2012; Hunter et al., 1990; Koh et al., 2009; Petersen et al., 1998; Salinas et al., 2005; Thurley and Ng, 2008), porosity identification (Ghiasi-Freer et al., 2012), and froth monitoring (Aldrich et al., 2010).

One of the first attempts at using digital image analysis in mining can be found in Oestreich et al. (1995), in which they reported using a color

<sup>\*</sup> Corresponding author.

E-mail addresses: [clperez@ing.uchile.cl](mailto:clperez@ing.uchile.cl) (C.A. Perez), [jsaravia@ing.uchile.cl](mailto:jsaravia@ing.uchile.cl) (J.A. Saravia), [canavarr@ing.uchile.cl](mailto:canavarr@ing.uchile.cl) (C.F. Navarro), [dschulz@ing.uchile.cl](mailto:dschulz@ing.uchile.cl) (D.A. Schulz), [cararave@ing.uchile.cl](mailto:cararave@ing.uchile.cl) (C.M. Aravena), [fgaldame@ing.uchile.cl](mailto:fgaldame@ing.uchile.cl) (F.J. Galdames).

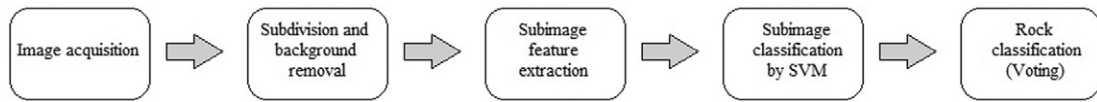


Fig. 1. Main steps from image acquisition to rock classification.

sensor system based on a color vector angle to estimate the composition of a mixture of two minerals, chalcopyrite and molybdenite. Perez et al. (1999, 2012) and Casali et al. (2001) classified seven types of lithologies, extracting color (Haralick, 1979; Ojala et al., 1996; Paclik et al., 2005; Singh et al., 2010), and geometric features from the rock images. In these approaches feature selection using a genetic algorithm was performed and a multi-layer neural network was trained to classify. The method included a rock segmentation scheme based on binarization and morphological operators. Tessier et al. (2007) presented an on-line automatic ore composition estimator mounted on a conveyor belt in a laboratory. They used color and texture features based on Wavelets and Principal Component Analysis (PCA) to train three different support vector machines (SVMs) to classify five rock types into three different classes, showing promising results on both dry and wet rock images. In Perez et al. (2011b), a voting scheme using segmentation and boundary detection was introduced to improve previous results. Preliminary results using Gabor features in only one database with a small partition of three subsets were presented in Perez et al. (2012).

This paper presents a new method for rock lithological classification based on multi-scale texture feature extraction, sub-image classification and voting on all sub-images within the rock contour. First, each image is broken into sub-images and then a feature extraction process is applied to each sub-image using Gabor filters of different scales and orientations. These features are then used as inputs to an SVM classifier for estimating rock type for each sub-image. Finally, the rock contour information is used to classify each rock by a vote among all sub-images that fall within the contour, significantly improving classification accuracy.

Results are compared advantageously with previously published methods on the same databases.

## 2. Methods and materials

The proposed method consists of several steps shown in the block diagram of Fig. 1. The main steps are image subdivision, sub-image feature extraction based on multiple scales and multiple orientation Gabor filters, sub-image classification based on SVM, and rock classification based on voting among sub-images that fall within the rock contour.

### 2.1. Image subdivision

Following the same process proposed in Tessier et al. (2007), and using the same image database, the images of  $1024 \times 1376$  pixels are divided into 512 sub-images of  $64 \times 43$  pixels. Each sub-image represents  $1.5 \text{ cm}^2$  and is considered to be the main processing unit for the classification process. Fig. 2 shows (a) an original image from the database and (b) another image composed of 512 sub-images of the same rock type after the background is removed.

Another experiment was performed on a new database composed of five rock types. Each image of size  $2048 \times 1536$  pixels was subdivided into 1024 sub-images. Fig. 2 shows (c) an image of rhyolitic diatreme rocks on the conveyor belt and (d) a subset of the sub-images obtained from (c) after background removal.

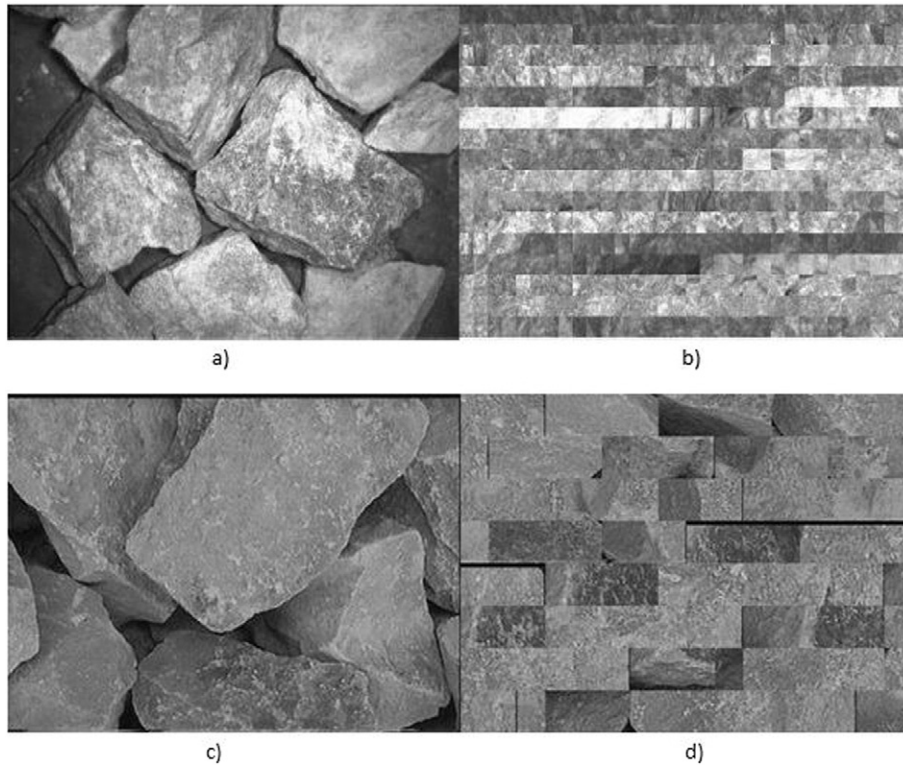
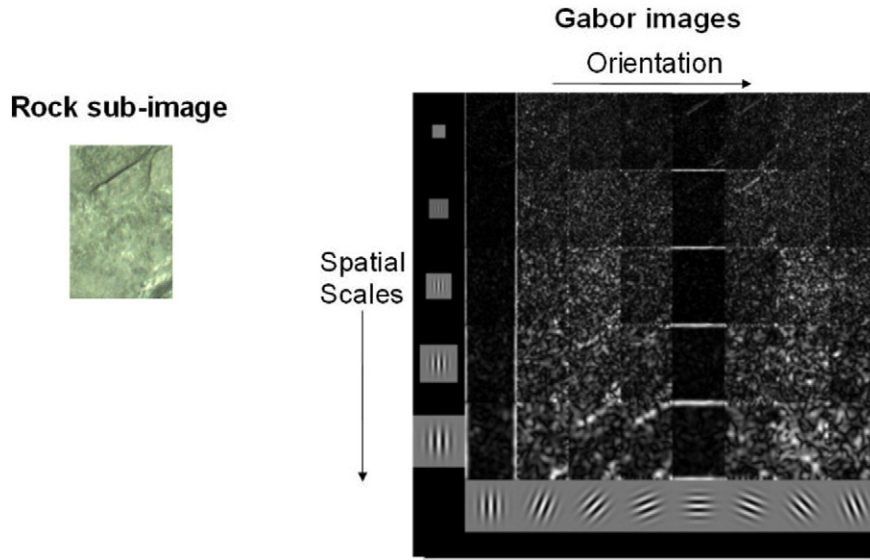


Fig. 2. Example of a group of gabbro rocks (a) on the conveyor belt and (b) a composed image of sub-images after removing the background. Figure (a) of  $1024 \times 1376$  pixels is divided into sub-image of  $64 \times 43$  pixels each of which represents a surface of  $1.5 \text{ cm}^2$ . (c) Image of rhyolitic diatreme rocks on the conveyor belt. (d) Sub-images obtained from (c) after background removal. Figure (c) has a size of  $2048 \times 1536$  pixels, and each sub-image of  $64 \times 48$  pixels represents a surface of approximately  $0.57 \text{ cm}^2$ .



**Fig. 3.** Example of Gabor filters applied to a rock sub-image for texture feature extraction. The effect of the application of the Gabor filters to the sub-image is shown for the five spatial scales (columns) and eight orientations (rows).

## 2.2. Sub-image feature extraction

Features were extracted from each sub-image using Gabor filters (Gabor, 1946), 8 orientations, and 5 spatial scales (Perez et al., 2011a; Cament et al., 2014). A Gabor filter in 2D is a sinusoidal function modulated by a Gaussian envelope, with orientation  $u$  and spatial scale  $v$ , and is defined as follows:

$$\Psi_{u,v}(x,y) = \frac{|\vec{k}|^2}{\sigma^2} \exp\left(\frac{|\vec{k}|^2 - |\vec{r}|^2}{2\sigma^2}\right) \left[ e^{i\vec{k}\vec{r}} - e^{-\sigma^2/2} \right], \quad (1)$$

where

$$\vec{r} = (x,y)^T \text{ and } \vec{k} = \frac{k_{\max}}{f} e^{i\pi u/8}.$$

For this work, we used eight orientations,  $0 \leq u \leq 7$  and five spatial scales,  $1 \leq v \leq 5$ ,  $\sigma = 2\pi$ ,  $k_{\max} = \pi/2$ , and  $f = \sqrt{2}/2$ , which are the best suited due to the sub-image sizes (Perez et al., 2011b). Fig. 3 shows an example of these Gabor filters applied to a rock sub-image.

The Gabor features are obtained from each sub-image by convolution of the image  $I(x,y)$  with the Gabor kernel as:

$$G_{u,v}(x,y) = I(x,y) * \Psi_{u,v}(x,y). \quad (2)$$

The Gabor transformation is a complex function which can be separated in magnitude  $A_{u,v}(x,y)$  and phase  $\theta_{u,v}(x,y)$ , and can be rewritten as follows:

$$G_{u,v}(x,y) = A_{u,v} \exp(i\theta_{u,v}(x,y)). \quad (3)$$

Eq. (3) is a complex representation of the Gabor transformation of the sub-image from which a feature vector is created. We compute the mean  $\mu_{u,v}$  and standard deviation  $\sigma_{u,v}$  for the magnitude  $A_{u,v}(x,y)$ , and with these measures we form a feature vector of a length two times the number of filters, for a color (or grayscale) channel  $c$ . As in HSV and RGB, there are three color channels; the feature vector for each sub-image is obtained by concatenation of the three feature vectors from the three channels. A total of 80 features are extracted from each color component (5 scales and 8 orientations with  $\mu_{u,v}$  and  $\sigma_{u,v}$ ). As a consequence a total of 240 features are considered in the feature vector representing each sub-image.

## 2.3. SVM classifier

After the feature extraction, the feature vector for each sub-image is used as the input to the classifier. The SVM classifier has become very popular within the machine learning community due to its great

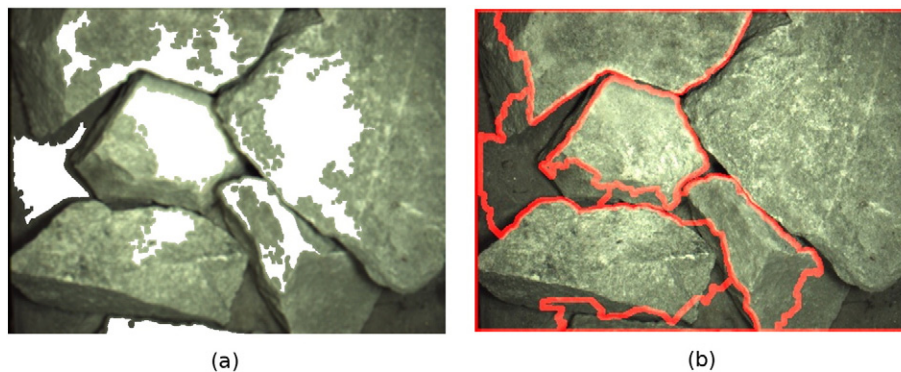


**Fig. 4.** Example of the rock segmentation obtained by applying the Watershed algorithm. (a) Initial markers or seeds (white). (b) Final segmentation of the rocks. The images of  $1024 \times 1376$  pixels represent a surface of  $768 \text{ cm}^2$ .

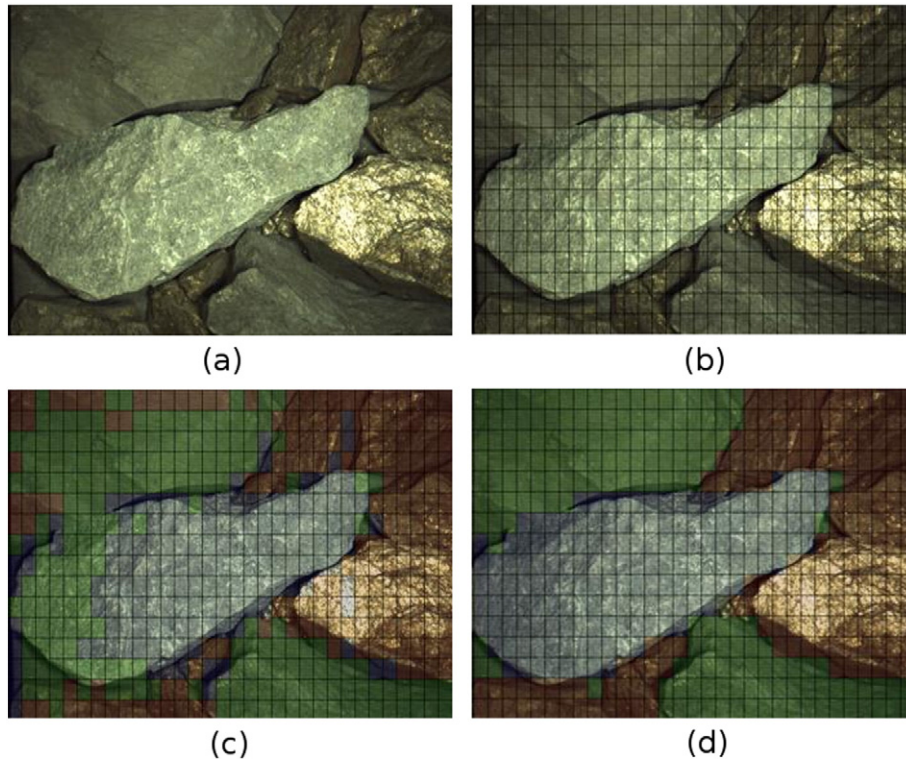


**Fig. 5.** Example of the rock type classification algorithm. (a) Initial image of 1024 × 1376 pixels. (b) Image divided into sub-images of 64 × 43 pixels, each of which represents a surface of 1.5 cm<sup>2</sup>. (c) SVM classification of each sub-image. (d) Final classification after segmentation and voting.

classification potential (Meyer et al., 2003). The SVM maps input vectors in a non-linear transformation to a high-dimensional space where a linear decision hyper-plane is constructed for class separation (Cortes and Vapnik, 1995). Although the SVM was originally designed to solve a two-class problem, the extension for the separation of three or more classes is straightforward. The 240 features were the input to the SVM classifier.

2.4. Contour detection and background removal

The contour detection and background removal are performed using the Watershed transform (Beucher and Lantuejoul, 1979) to create border maps with the background and boundaries as was explained in Perez et al. (2011b). The watershed transform is a segmentation method based on mathematical morphology, using a region-based segmentation approach. It is based on the idea of a landscape or topographic relief which is flooded by water (Roerdink and Meijster, 2001). In this

study the initial seeds were generated using morphological operations with a smoothing kernel of size 5 × 5 pixels, opening by reconstruction, closing by reconstruction and regional maxima (Soille, 2003). After the creation of the seeds, the watershed transform was applied on the image using the seeds as the markers. Fig. 4 shows (a) the initial markers (seeds) used as input to the Watershed algorithm, and (b) the final segmentation.

Once the border map is obtained, blobs are defined as areas in the image that fall within a closed loop. A threshold is applied for discarding background and border sub-images using the number of edge pixels in the sub-images. All sub-images that were not discarded as background or borders were then grouped according to the border map provided by the rock segmentation. Once the SVM had classified these sub-images individually, a voting process was applied to each group in order to eliminate possible classification errors. In this work a simple voting method was chosen in which all sub-images within a group were classified according to the most predominant rock type present

**Table 1**  
Classification results (accuracy) for dry rock images using Wavelet-PCA and Gabor features with an SVM classifier for the first experiment on the nickel mine database (Tessier et al., 2007). Results are shown for the test set based on sub-image classification (3rd and 7th columns) and adding voting among sub-images within the rock contour (5th and 9th columns).

Features	Wavelet-PCA				Gabor			
	Sub-image		Voting		Sub-image		Voting	
Sets	Training [%]	Test [%]						
1	90.54	77.24	99.22	86.80	95.10	90.78	96.44	96.24
2	85.61	81.28	92.71	90.76	95.44	90.37	96.20	94.49
3	90.93	79.25	98.62	86.80	95.33	90.37	96.20	94.65
4	87.65	79.72	98.32	94.87	94.74	91.36	96.27	96.30
5	85.12	80.44	93.86	92.96	95.28	90.35	96.20	94.65
Average	87.97	79.59	96.55	90.44	95.18	90.65	96.26	95.27
Std dev	2.70	1.52	3.02	3.63	0.27	0.44	0.10	0.92

**Table 2**  
Classification results (accuracy) for wet images using Wavelet-PCA and Gabor features with an SVM classifier for the first experiment on the nickel mine database (Tessier et al., 2007). Results are shown for the test set based on sub-image classification (3rd and 7th columns) and adding voting among sub-images within the rock contour (5th and 9th columns).

Features	Wavelet-PCA				Gabor			
	Sub-image		Voting		Sub-image		Voting	
Sets	Training [%]	Test [%]						
1	84.87	83.20	92.25	92.80	90.66	85.15	94.29	93.07
2	85.92	82.50	93.67	91.70	91.46	84.87	95.65	92.63
3	86.75	81.38	93.57	90.19	91.45	85.12	95.63	92.31
4	84.65	83.50	92.57	93.07	90.16	85.99	94.19	93.75
5	86.48	81.42	93.57	90.25	91.45	85.18	95.63	92.34
Average	85.73	82.40	93.13	91.60	91.04	85.26	95.08	92.82
Std dev	0.94	0.98	0.66	1.63	0.60	0.43	0.77	0.60

in that particular group. Fig. 5 shows an example of the complete classification algorithm where: (a) the original image, (b) is subdivided in sub-images, and (c) that are classified by the SVM classifier independently. (d) Finally, after segmentation and voting, classification errors are greatly reduced.

## 2.5. Databases and experiments

In this paper we report performing three experiments with three different databases. In the first experiment, we used images from a database of five types of rocks that had been used in previous publications (Tessier et al., 2007; Perez et al., 2011b), making comparison of our results with those of previous work possible. In this database, images from a nickel mine were acquired from five ore types: massive sulfide (MS), disseminated sulfide (DS), net textured sulfide (NT), gabbro (G), and peridotite (P). The database was organized into three classes according to rock grindability. MS was assigned to the soft class, DS and NT to the medium class, and G and P to the hard class (Tessier et al., 2007). Each digital image of  $1024 \times 1376$  pixels was divided into 512 sub-images of  $64 \times 43$  pixels. Each sub-image captured the relevant color and texture features of the rock (Tessier et al., 2007).

The Gabor features were extracted from each sub-image. This database contains images half of which are dry, and half wet rock images. The background and edges from each rock were eliminated to have sub-images composed of the core of each rock. The training set was made up of 50 images with 512 sub-images each (a total of 25,600 sub-images). We used a five-fold cross-validation to find the best parameters for the SVM. After determining the SVM parameters, the result of training was determined with a different set of 50 images having 512 sub-images each (25,600 sub-images). For testing we used a different set of 265 images in which each image was divided into 512 sub-images. As in the case of training, background and edges were eliminated to yield a test set of 120,213 sub-images.

In the second experiment, ore samples from a copper mine in Chile were used (Casali et al., 2001; Perez et al., 1999). This database is composed of seven types of rocks that can be grouped into seven lithological classes: Andesite (AN), Tourmaline Breccia (BxT), Dacitic Diatreme (CHDA), Rhyolitic Diatreme (CHRiol), Porphyritic Dykes (PDL), Granodiorites (GDCC), and Other Breccias (BxTo). The database was built using color digital images obtained with a conventional CCD-NTSC camera and a frame grabber. We used 420 digital images, each one showing between 20 and 40 rocks, in BMP format, each having  $640 \times 480$  pixels. The ore particle size was  $100\% - 17.8 \text{ cm} + 3.8 \text{ cm} (-7'' + 1.5'')$ . As in experiment 1, the background and edges from each rock were eliminated to have sub-images composed of the core of each rock. The training set contained 210 images with 128 sub-images each (a total of 21,070 sub-images). We used a five-fold cross-validation to find the best parameters for the SVM. For testing we used a different set of 210 images in which each image was divided into 128 sub-images. As in the case of training, background and edges were eliminated to yield a test set of 21,880 sub-images.

The third experiment was performed on a new database composed of a subset of five rock types used in the second experiment: Andesite

**Table 4**

Classification results (accuracy) for the copper mine database (Casali et al., 2001) with 7 lithological classes for the test sets using Gabor and Wavelet PCA features and an SVM Classifier (second experiment). Results are shown for the test set based on sub-image classification (3rd column) and adding voting among sub-images within the rock contour (5th column).

Method	Sub-images		Voting	
	Training [%]	Test [%]	Training [%]	Test [%]
Method	Sub-images		Voting	
Gabor	76.20	66.00	93.30	82.40
Wavelet PCA	48.60	40.83	77.87	65.13

(AN), Dacitic Diatreme (CHDA), Rhyolitic Diatreme (CHRiol), Porphyritic Dykes (PDL), and Other Breccias (BxTo). The database was built using color digital images obtained with a digital IP-camera. We used 200 digital images, each one showing between 10 and 30 rocks, in JPG format and each having  $2048 \times 1536$  pixels. As in experiment 1, the background and edges from each rock were eliminated to have sub-images built with the core of each rock. The training set was composed of 100 images with 1024 sub-images each (a total of 102,400 sub-images). We used a five-fold cross-validation to find the best parameters for the SVM. For testing we used a different set of 100 images in which each image was divided into 1024 sub-images. As in the training set, background and edges were eliminated to yield a test set of 102,400 sub-images.

The image subdivision, feature extraction, SVM classifier and voting algorithms were implemented using Matlab. Rock segmentation was implemented in C++ using the OpenCV library for image processing.

Results were compared with a Wavelet-PCA feature extraction method previously published in Tessier et al. (2007) and Perez et al. (2011b). Wavelets extract texture features (Mallat, 1989; Murtagh and Starck, 2008), and the PCA extracts color features. A feature selection method based on Mutual Information was used to select 14 features from 36 (30 wavelets and 6 PCAs). The classifier was also an SVM, but instead of using only one classifier, a cascade with three classifiers on the first layer and one classifier on a second layer was used.

## 3. Results and discussion

### 3.1. Methods results

Table 1 shows the classification accuracy in the first experiment, in which Wavelet-PCA features were used on dry rock images. It can be observed that the average accuracy for the five sets used in the test database reached 79.59%. Results using the Wavelet-PCA features can be significantly improved, reaching an average classification accuracy of 90.44% if voting among all sub-images that fall within the rock contour is employed, as we propose in our method. Table 1 also shows results for Gabor features on dry rock images. It can be observed that results for individual sub-images reached an average classification accuracy of 90.65% on the five testing subsets. Table 1 also shows that results with Gabor features improved classification accuracy to an average of 95.27% on the five testing subsets when voting among all sub-images

**Table 3**  
Confusion matrices for the second experiment on the copper mine database (Casali et al., 2001) with 7 lithological classes for our proposed method using Gabor features for the training and test sets.

Sets Type	Training							Test						
	C1	C2	C3	C4	C5	C6	C7	C1	C2	C3	C4	C5	C6	C7
Andesite	3820	0	0	0	0	0	0	3737	0	0	0	40	36	0
Dacitic Diatreme	0	3489	147	115	0	2	58	0	2841	246	512	0	3	224
Rhyolitic Diatreme	0	259	3491	33	0	2	46	0	248	3212	188	0	145	36
Porphyritic Dykes	0	274	62	3341	0	41	111	0	864	174	2319	0	207	267
Other Breccias	0	0	0	0	3816	0	0	0	0	0	0	3824	0	0
Granodiorites	0	3	6	7	0	3513	287	0	53	96	213	2	3172	285
Tourmaline Breccia	0	138	41	26	11	135	3463	0	120	93	141	79	429	2951

**Table 5**

Confusion matrices for the copper mine database (third experiment) with 5 lithological classes for our proposed method using Gabor features for the training and test sets.

Sets Type	Training					Test				
	C1	C2	C3	C4	C5	C1	C2	C3	C4	C5
Andesite	5088	17	7	13	107	4428	34	11	110	380
Dacitic Diatreme	90	8997	159	713	0	123	9114	247	652	1
Rhyolitic Diatreme	95	365	8568	293	72	175	281	8233	479	79
Porphyritic Dykes	275	2769	396	6021	83	329	2618	474	6167	115
Other Breccias	49	0	49	37	7985	87	6	99	63	7632

that fall within the rock contour was employed. The overall classification accuracy when Gabor features and voting were used improved by almost 15% relative to previously published methods on the same database. Table 1 also shows the standard deviations measured for the five testing sets. The standard deviation was small (0.92%) in the case of voting, meaning that the five different partitions represented the different rock types present in the training set well.

Table 2 shows the results of the Wavelet-PCA feature method when tested on wet rock images. The average classification accuracy for the Wavelet-PCA method in the test database reached an average of 82.40% on the five sets. It can be observed that by adding our voting process for all sub-images within the rock contour, the average classification accuracy improved significantly to 91.60%. Table 2 also shows the classification accuracy for our proposed method based on Gabor features for wet rock images. The average classification accuracy using sub-images reached 85.26% on the test set. This result improved to 92.82% when voting among all sub-images that fell within the rock contour was included.

The overall classification accuracy improved more than 10% relative to previously published methods on the same database. Table 2 also shows the standard deviations for the five testing sets. In the case of voting, the standard deviation was 0.60% which means that each partition was well represented by the training set. In Tables 1 and 2 it can be observed that our proposed method based on Gabor filter and voting yielded significantly better results than the previously published Wavelet PCA method on dry and wet rock images. Comparing results of both features with voting in Tables 1, it can be seen that an improvement of 1.3% in classification accuracy is obtained by using Gabor features instead of Wavelet-PCA features in dry rocks. Also, comparing the performance of both features with voting in Tables 2, it is evident that an improvement in classification accuracy of 1.22% is obtained by using the Gabor method instead of the Wavelet-PCA in wet rocks.

Dust covering the rocks may impact the results of methods based on image analysis within the visual light range (400–700 nm). Classification accuracy on wet rock images represents a possible solution when dust removal from the rock surface can be performed using water. An alternative is to perform the dust removal far away from the image acquisition point, which could be several kilometers away in underground mines, so that rocks would arrive dry to the image acquisition point.

With the purpose of analyzing the performance of our method, confusion matrices were computed to study cross-class errors. A confusion matrix shows on its rows the number of samples for each class (groundtruth) and in the columns the number of samples labeled as the corresponding class (predicted). A method with no errors would classify all samples along the diagonal of the confusion matrix, while a large value on a cell outside the diagonal indicates a large number of errors in the predicted class relative to the groundtruth. Table 3 shows the confusion matrices for the copper mine database in the training and testing sets. A lower performance on the Porphyritic Dykes class (PDL, fourth class), in both the training and testing sets can be observed.

Table 4 shows the overall classification accuracy for the copper mine database (seven classes) reaching 82.40% in the test set using our Gabor proposed method. This result is 17% higher than the result obtained

with the Wavelet-PCA method on the same test database from the copper mine database using our proposed voting method. This result is even higher (26%) if we compare our results with Gabor features and Wavelet-PCA without our proposed voting method.

Tables 5 shows the confusion matrices for the second copper mine database in the training and testing sets (third experiment). As in the second experiment, it can be observed that the lower performance occurs on the Porphyritic Dykes class (PDL, fourth class), in both the training and testing sets.

Table 6 shows the overall classification accuracy for the second copper mine database (five classes) reaching 84.8% in the test set using our Gabor proposed method. This result is 9.11% higher than the result obtained with the Wavelet-PCA method on the same test database from the copper mine database using our proposed voting method. This result is even higher (33.95%) if we compare our results with Gabor features and Wavelet-PCA without our proposed voting method.

### 3.2. Feature selection using mutual information

Entropy  $H$  is a measure of the uncertainty of random variables. Let  $\chi$  be, or represent, a discrete random variable. The entropy of  $\chi$  is defined as:

$$H(x) = -\sum_{x \in \chi} p(x) \log(p(x)). \quad (4)$$

The mutual information,  $MI$ , between two variables,  $x$  and  $y$ , is defined based on their joint probabilistic distribution  $p(x,y)$  and the respective marginal probabilities  $p(x)$  and  $p(y)$  as:

$$MI(x,y) = \sum_{i,j} p(x_i, y_j) \log \frac{p(x_i, y_j)}{p(x_i)p(y_j)}. \quad (5)$$

The Conditional Mutual Information Maximization (CMIM) criterion (Fleuret and Guyon, 2004; Wang and Lochovsky, 2004) considers the  $MI$  between the candidate feature variable  $F_i$  and the output class  $c$  given each one of the variables in the set  $S$ , separately. It allows preserving a certain trade-off between the prediction of  $F_i$  with respect to the output and the independence of candidate features with each single variable

**Table 6**

Classification results (accuracy) for the copper mine database with 5 lithological classes for the test sets using Gabor and Wavelet PCA features and an SVM Classifier (third experiment). Results are shown for the test set based on sub-image classification (3rd column) and adding voting among sub-images within the rock contour (5th column).

Method	Sub-images		Voting	
	Training [%]	Test [%]	Training [%]	Test [%]
Method	Sub-images	Test [%]	Voting	Test [%]
	Training [%]	Test [%]	Training [%]	Test [%]
Gabor	70.50	66.90	86.80	84.80
Wavelet PCA	36.71	32.95	84.59	75.69

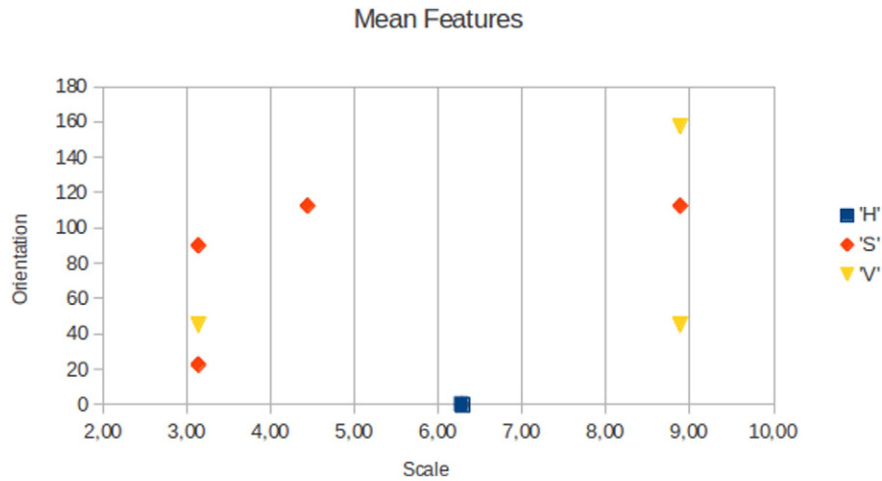


Fig. 6. Selected mean features, spatial scale ( $k_{nu}$ ) vs. orientations (°).

previously selected. CMIM considers that feature  $F_i$  is relevant only if it provides high information about  $c$  and this information is not contained in any of the variables already selected.

$$CMIM = \left\{ \begin{array}{l} \arg \max_{f_i \in F} \{MI(f_i; c)\} \text{ for } S = 0 \\ \arg \max_{f_i \in S} \{ \min_{f_j \in S} MI(f_i; c/f_j) \} \text{ for } S \neq 0 \end{array} \right\} \quad (6)$$

We performed a feature selection over the 240 Gabor features using the CMIM measure. Thus, we selected those features with highest CMIM value.

The main goal of feature selection is to select a small number of features that can carry as much information as possible. This goal can be interpreted as maximizing the joint MI (JMI),  $I(F_1, \dots, F_k; C)$ , for  $k$  features. It can be shown that  $I(F_1, \dots, F_k; C) - I(F_1, \dots, F_{k-1}; C) = I(F_k; C | F_1, \dots, F_{k-1})$  in which  $I(F_k; C | F_1, \dots, F_{k-1})$  is conditional MI (CMI), which quantifies the shared information between  $F_k$  and  $C$ , given features  $F_1, \dots, F_{k-1}$ . CMI provides a useful way to select a new feature  $F_k$ , since both, the relationship with other features and its individual information are expressed. Thus, features can be selected one by one for the feature set through an iterative process. In each step, a feature  $F^*$  is selected only if  $I(F^*; C | F_1, \dots, F_{k-1})$  is the highest given that  $k - 1$  features are already selected.

We used this method to determine a ranking of color–texture features, and then we took different subsets to classify the rocks with a fewer number of features, identifying the most useful features for our classification problem. Results show that using only 17 features, which

are less than 10% of the original set of features, the classification rate on the rock database with 5 different classes (Copper) reached almost the same results as in the case with the full set of features. Therefore, we can identify which the best features are. Figs. 6 and 7 show the selected features of the mean and standard deviation measures respectively. Our results show that the smallest spatial scale (Gabor factor  $k_{nu} = 2.22$ ) does not provide relevant information because those features were not selected. The mean measures show that the orientations are complementary over the different scales. For example, the second scale (for  $k_{nu} = 3.14$ ) is represented only with orientations of 22.5°, 45° and 90°; the third ( $k_{nu} = 4.44$ ) has only 112.5°; the fourth scale ( $k_{nu} = 6.28$ ) is represented only with 0° orientation; and in the fifth scale ( $k_{nu} = 8.89$ ) the orientations are 45°, 112.5° and 157.5°. The orientation 67.5° does not provide any relevant feature, on any scale. For the standard deviation measures, the first and third scales do not provide any relevant data. Meanwhile, the fourth and fifth scales are represented in 0°, 22.5°, 45° and 112.5°, 135°, 157.5° orientations respectively; and the second scale is represented by 45°, 67.5° and 112.5°. The orientation 90° does not provide any relevant feature, on any scale.

By using MI to select the most important Gabor features, we can extract qualitative information about the classification process in order to highlight the relevant features for performing rock classification. The selected features shown in Figs. 6 and 7 correspond to the most relevant information to perform rock classification by using Gabor color–texture features on the database. Selected features give us some important clues regarding texture and color information for improving image-

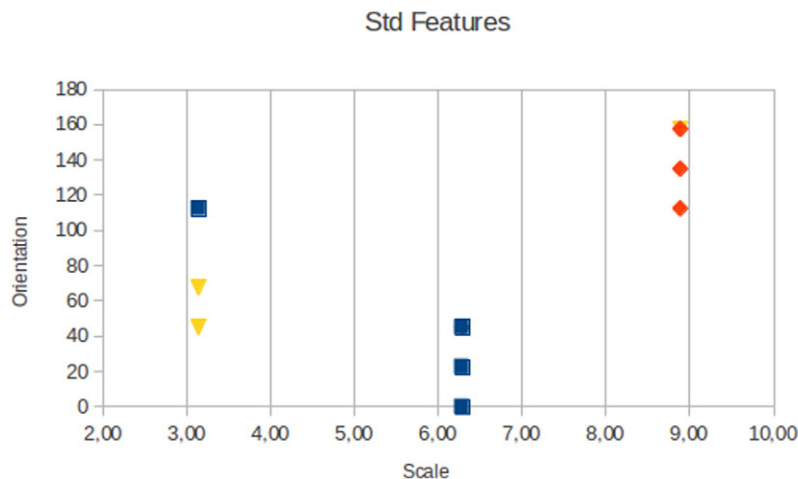


Fig. 7. Selected standard deviation features, spatial scale ( $k_{nu}$ ) vs. orientations (°).

processing based algorithms for rock lithological classification, such as scales and orientations necessary to extract meaningful information. Nevertheless, this information in its current form, does not correlate with other meaningful data such as grain size, or degree of alteration. The results show that the proposed method can differentiate among ore classes for which the method was trained.

#### 4. Conclusions

A new method for remote rock lithological classification is proposed in this paper. The method is based on image subdivision into sub-images and a Gabor feature extraction using 5 different spatial scales with 8 orientations applied to each sub-image. Then, each sub-image is classified using an SVM classifier. Each rock is classified using contour information making all sub-images that fall within the contour vote for the rock class. We tested the proposed method using two databases; one from a nickel mine used previously (Tessier et al., 2007; Perez et al., 2011b) and a second database from a copper mine with seven different rock types. Our results were compared to those previously published (Wavelet-PCA) on the same databases.

Classification accuracy of our Gabor based method showed significantly better performance on both databases compared to previously published results. Our results are almost 15% better on the dry rock images and 20% better on the wet rock images for the three classes of the nickel mine, nearly 17% better on the seven classes of the copper mine database, and 9.11% better on the reduced five classes of the copper mine database. The classification performance was almost 10% lower on the copper mine database compared to the nickel mine database. This could be explained by there being seven (or five) classes in the copper mine database compared with having only three classes in the nickel mine database.

Results obtained in this work are very promising, and the importance of remote ore sorting has already been discussed in many previous publications. Nevertheless, further developments in a pilot plant are required to validate the methods in an industrial environment. We want to emphasize that the proposed method could be used to optimize mill operation by having remote information online about the grindability of rocks that are being fed into the mill. A significant amount of energy could be saved in the grinding process by having an appropriate sensor to classify the rock types.

#### Acknowledgments

We would like to thank Prof. Carl Duchesne from Université Laval, Canada, for providing us part of the rock database used in Tessier et al. (2007). This research has been funded by FONDEF project D0811060 and FONDECYT 1120613 from Conicyt, by the Department of Electrical Engineering and the Advanced Mining Technology Center (AMTC), Universidad de Chile.

#### References

Aldrich, C., Marais, C., Shean, B.J., Cilliers, J.J., 2010. Online monitoring and control of froth flotation systems with machine vision: a review. *Int. J. Miner. Process.* 96 (1–4), 1–13.

Al-Batah, M.S., Isa, N.A.M., Zamli, K.Z., Sani, Z.M., Azizi, K.A., 2009. A novel aggregate classification technique using moment invariants and cascaded multilayered perceptron network. *Int. J. Miner. Process.* 92 (1–2), 92–102.

Al-Thyabat, S., Miles, N.J., Koh, T.S., 2007. Estimation of the size distribution of particles moving on a conveyor belt. *Miner. Eng.* 20 (1), 72–83.

Andersson, T., Thurlay, M., Carlson, J., 2012. A machine vision system for estimation of size distributions by weight of limestone particles. *Miner. Eng.* 25, 38–46.

Baykan, N.A., Yilmaz, N., 2010. Mineral identification using color spaces and artificial neural networks. *Comput. Geosci.* 36 (1), 91–97.

Beucher, S., Santuejoul, C., 1979. Use of watersheds in contour detection. *International Workshop on Image Processing, Real-Time Edge and Motion Detection/Estimation, Rennes*, pp. 17–21.

Bianconi, F., González, E., Fernández, A., Saetta, S., 2012. Automatic classification of granite tiles through colour and texture features. *Expert Syst. Appl.* 39, 11212–11218.

Buckingham, L., Dupont, J.-F., Stieger, J., Blain, B., Brits, C., 2011. Improving energy Efficiency in Barrick grinding circuits. *Proceedings of 5th International Conference on Autogenous and Semi-autogenous Grinding Technology (SAG2011)* (13 pp.).

Cament, L.A., Castillo, L.E., Perez, J.P., Perez, C.A., 2014. Fusion of local normalization and Gabor entropy weighted features for face identification. *Pattern Recogn.* 47, 568–577.

Casali, A., Gonzalez, G., Vallebuona, G., Perez, C., Vargas, R., 2001. Grindability soft-sensors based on lithological composition and on-line measurements. *Miner. Eng.* 14 (7), 689–700.

Cortes, C., Vapnik, V., 1995. Support-vector networks. *Mach. Learn.* 20 (3), 273–297.

Chatterjee, S., Bandopadhyay, S., Machuca, D., 2010a. Ore grade prediction using a genetic algorithm and clustering based ensemble neural network model. *Math. Geosci.* 42 (3), 309–326.

Chatterjee, S., Bhattacharjee, A., Samanta, B., Pal, S.K., 2010b. Image-based quality monitoring system of limestone ore grades. *Comput. Ind.* 16 (5), 391–408.

Chatterjee, S., 2012. Vision-based rock-type classification of limestone using multi-class support vector machine. *Appl. Intell.* 1–14.

De Magalhães, F.N., Tavares, L.M., 2014. Rapid ore breakage parameter estimation from a laboratory crushing test. *Int. J. Miner. Process.* 126, 49–54.

Fleuret, F., Guyon, I., 2004. Fast binary feature selection with conditional mutual information. *J. Mach. Learn. Res.* 5, 1531–1555.

Gabor, D., 1946. Theory of communication. *J. Inst. Electr. Eng.* 93 (3), 429–457.

Gerson, A.R., Smart, R.S.C., Li, J., Kawashima, N., Weedon, D., Triffett, B., Bradshaw, D., 2012. Diagnosis of the surface chemical influences on flotation performance: copper sulfides and molybdenite. *Int. J. Miner. Process.* 106–109, 16–30 (20 May).

Ghiasi-Freer, J., Soleimanpour, I., Kadkhodaie-Ilkhchi, A., Ziaii, M., Sedighi, M., Hatampour, A., 2012. Semi-automated porosity identification from thin section images using image analysis and intelligent discriminant classifiers. *Comput. Geosci.* 45, 36–45.

Guyot, O., Monredon, T., LaRosa, D., Broussaud, A., 2004. VisioRock, an integrated vision technology for advanced control of comminution circuits. *Miner. Eng.* 17 (11–12), 1227–1235.

Haralick, R.M., 1979. Statistical and structural approaches to texture. *Proc. IEEE* 67 (5), 786–804.

Hunter, G.C., McDermott, C., Miles, N.J., Singh, A., Scoble, M.J., 1990. A review of image analysis techniques for measuring blast fragmentation. *Min. Sci. Technol.* 11 (1), 19–36.

Jungmann, M., Kopal, M., Clauser, C., Berlage, T., 2011. Multi-class supervised classification of electrical borehole wall images using texture features. *Comput. Geosci.* 37 (4), 541–553.

Koh, T.K., Miles, N.J., Morgan, S.P., Hayes-Gill, B.R., 2009. Improving particle size measurement using multi-flash imaging. *Miner. Eng.* 22 (6), 537–543.

Köse, C., Alp, I., Ikbaz, C., 2012. Statistical methods for segmentation and quantification of minerals in ore microscopy. *Miner. Eng.* 30, 19–32.

Mallat, S.G., 1989. A theory for multiresolution signal decomposition: the wavelet representation. *IEEE Trans. Pattern Anal. Mach. Intell.* 11 (7), 674–693.

Mat Isa, N.A., Sani, Z., Subhi Al-Batah, M., 2011. Automated Intelligent real-time system for aggregate classification. *Int. J. Miner. Process.* 100 (1–2), 41–50 (8 July).

Meyer, D., Leisch, F., Hornik, K., 2003. The support vector machine under test. *Neurocomputing* 55 (1–2), 169–186.

Morrell, S., 2004. Predicting the specific energy of autogenous and semi-autogenous mills from small diameter drill core samples. *Miner. Eng.* 17 (3), 447–451.

Murtagh, F., Starck, J.L., 2008. Wavelet and curvelet moments for image classification: application to aggregate mixture grading. *Pattern Recogn. Lett.* 29 (10), 1557–1564.

Mwanga, A., Lamberg, P., Rosenkranz, J., 2015. Comminution test method using small drill core samples. *Miner. Eng.* 72, 129–139.

Oestreich, J.M., Tolley, W.K., Rice, D.A., 1995. The development of a color sensor system to measure mineral compositions. *Miner. Eng.* 8 (1–2), 31–39.

Ojala, T., Pietikainen, M., Harwood, D., 1996. A comparative study of texture measures with classification based on feature distributions. *Pattern Recogn.* 29 (1), 51–59.

Paclik, P., Verzakov, S., Duin, R.P.W., 2005. Improving the maximum-likelihood co-occurrence classifier: a study on classification of inhomogeneous rock images. *Proceedings of the 14th Scandinavian conference on Image Analysis SCIA'05* 3540, pp. 998–1008.

Perez, C., Casali, A., Gonzalez, G., Vallebuona, G., Vargas, R., 1999. Lithological composition sensor based on digital image feature extraction, genetic selection of features and neural classification. *Proceedings of the IEEE International Conference on Information Intelligence and Systems ICIS'99, Bethesda, MD, Oct.31-Nov.3*, pp. 236–241.

Perez, C.A., Cament, L.A., Castillo, L.E., 2011a. Methodological improvement on local Gabor face recognition based on feature selection and enhanced Borda count. *Pattern Recogn.* 44 (4), 951–963.

Perez, C.A., Estévez, P.A., Vera, P., Castillo, L.E., Aravena, C.M., Schulz, D.A., Medina, L.E., 2011b. Ore grade estimation by feature selection and voting using boundary detection in digital image analysis. *Int. J. Miner. Process.* 101 (1–4), 28–36.

Perez, C.A., Schulz, D., Vera, P., Navarro, C., Castillo, L., Saravia, J., 2012. Rock lithological classification based on Gabor filters and support vector machine. *XXVI International Mineral Processing Congress (IMPC 2012)*, New Delhi, India, September 24–28, p. 2012 (6 pp.).

Petersen, K.R.P., Aldrich, C., Van Deventer, J.S.J., 1998. Analysis of ore particles based on textural pattern recognition. *Miner. Eng.* 11 (10), 959–977.

Roerdink, J.B.T.M., Meijster, A., 2001. The watershed transform: definitions, algorithms and parallelization. *Fundam. Inform.* 41, 187–228.

Salinas, R.A., Raff, U., Farfan, C., 2005. Automated estimation of rock fragment distributions using computer vision and its application in mining. *IEE Proceedings on Vision, Image and Signal Processing* 2005 152(1), pp. 1–8.

Shang, C., Barnes, D., 2012. Support vector machine-based classification of rock texture images aided by efficient feature selection. *IEEE World Congress on Computational Intelligence (WCCI 2012)*, June, 10–15, 2012–Brisbane, Australia, pp. 1–8.

- Singh, N., Singh, T.N., Tiwary, A., Sarkar, K.M., 2010. Textural identification of basaltic rock mass using image processing and neural network. *Comput. Geosci.* 14 (2), 301–310.
- Singh, V., Rao, S., 2006. Application of image processing in mineral industry: a case study of ferruginous manganese ores. *Miner. Process. Ext. Metall.* 115 (3), 155–160.
- Soille, P., 2003. *Morphological Image Analysis: Principles and Applications*. 2nd ed. Springer, Berlin; New York (408 pp.).
- Tessier, J., Duchesne, C., Bartolacci, G., 2007. A machine vision approach to on-line estimation of run-of-mine ore composition on conveyor belts. *Miner. Eng.* 20 (12), 1129–1144.
- Thurley, M.J., Ng, K.C., 2008. Identification and sizing of the entirely visible rocks from a 3D surface data segmentation of laboratory rock piles. *Comput. Vis. Image Underst.* 111 (2), 170–178.
- Yildirim, B.G., Bradshaw, D., Powell, M., Evans, C., Clark, A., 2014. Development of an effective and practical Process Alteration Index (PAI) for predicting metallurgical responses of Cu porphyries. *Miner. Eng.* 69, 91–96.
- Wang, G., Lochovsky, F.H., 2004. Feature selection with conditional mutual information maximin in text categorization. *Proceedings of the Thirteenth ACM International Conference on Information and Knowledge Management*, pp. 342–349.